fractal and fractional

Article

Designing Hyperbolic Tangent Sigmoid Function for Solving the Williamson Nanofluid Model

Basma Souayeh [1,2,*] and Zulqurnain Sabir [3,4]

1 Department of Physics, College of Science, King Faisal University, P.O. Box 400, Al-Ahsa 31982, Saudi Arabia
2 Laboratory of Fluid Mechanics, Physics Department, Faculty of Sciences of Tunis, University of Tunis El Manar, Tunis 2092, Tunisia
3 Department of Mathematics and Statistics, Hazara University, Mansehra 21300, Pakistan
4 Department of Computer Science and Mathematics, Lebanese American University, Beirut 10999, Lebanon
* Correspondence: bsouayeh@kfu.edu.sa or basma.souayeh@gmail.com

Abstract: This study shows the design of the novel hyperbolic tangent sigmoid function for the numerical treatment of the Williamson nanofluid model (WNM), which is categorized as velocity, concentration, and temperature. A process of a deep neural network using fifteen and thirty neurons is presented to solve the model. The hyperbolic tangent sigmoid transfer function is used in the process of both hidden layers. The optimization is performed through the Bayesian regularization approach (BRA) to solve the WNM. A targeted dataset through the Adam scheme is achieved that is further accomplished using the procedure of training, testing, and verification with ratios of 0.15, 0.13, and 0.72. The correctness of the deep neural network along with the BRA is performed through the overlapping of the solutions. The small calculated absolute error values also enhance the accurateness of the designed procedure. Moreover, the statistical observations are authenticated to reduce the mean square error for the nonlinear WNM.

Keywords: Williamson nanofluid model; layers; fluid dynamics; chemical reactions; numerical solutions

check for updates

Citation: Souayeh, B.; Sabir, Z. Designing Hyperbolic Tangent Sigmoid Function for Solving the Williamson Nanofluid Model. *Fractal Fract.* **2023**, *7*, 350. https://doi.org/10.3390/fractalfract7050350

Academic Editors: Changjin Xu, Maoxin Liao, Peiluan Li and Carlo Cattani

Received: 3 January 2023
Revised: 12 April 2023
Accepted: 18 April 2023
Published: 25 April 2023

1. Introduction

Metal oxides or metal generally represent the nanoparticles (NPs), which show an outstanding constancy in the surface area. NPs represent the competence of the thermophysical phenomenon and heat transport (HT). The form, shape, and different NPs designate HT effects. There are various applications of non-Newtonian fluid (NNF) that have been studied in recent years with the impacts of thermal radiation and chemical reactions [1]. The classification of NNF is presented in two steps, dependent and independent of time. The Williamson nanofluid (WNF) is a well-known form of NNF, which comprises pseudo-plastic topographies [2,3]. Krishnamurthy et al. [4] proposed the chemical and heat properties by applying the WNF with a porous medium. Hayat et al. [5] proposed an HT system with WNF features. Waqas et al. [6] explored the thermophoresis performance with Brownian diffusion along with thermal radiation impacts. Bhatti et al. [7] studied radiant heat conduct by applying NNPs. Goud et al. [8] performed different simulations based on the radiation of magnetohydrodynamics. Pramod et al. [9] discussed the Soret impacts with a porous portable plate.

The WNF has a variety of applications such as blood circulation, plasma mechanics, and ice cream and crude oil processing. WNF conduction represents the pseudoplastic fluid. The diffusivity ratio and Lewis number have enormous implementations using the process of HT. Heat transfer along with the effects of the WNF pass over the peristaltic pumping, and the stretching medium has been examined by Sreenadh et al. [10]. S. Prasad et al. [11] provided a free WNF convection using the inclined channel with a relevant pattern of the magnetic field. Ayub et al. [12,13] discussed the heat/mass transport using the magnetized orthogonal/inclined magnetic field with the spinning disk. HT impacts and WNF, together with boundary layer construction, were studied by Nadeem et al. [14]. They proposed that by improving the parametric Williamson form, the amount of skin friction was reduced. Venkataramanaiah et al. [15] discussed the heat/mass transfer and the MHD effects using the WNF. They proposed that the flux of mass/heat transfer improves to upgrade the Williamson parameter. The inertial features with the microstructure using the magnetite ferrofluid of thermal conductivity kind of operative system is studied in Ref. [16]. The transfer of heat in with non-magnetic and magnetic NPs is reported in Ref. [17]. The morphological nanolayer effects on the hybrid nanofluids' flow are discussed by Qureshi et al. [18]. The mono/hybrid nanofluids dynamics, subject to magnetic field, activation energy, and a binary chemical reaction using the porous surfaces, is presented by Raza et al. [19]. The heat transfer deterioration of supercritical water flowing in a vertical tube through the suspension of alumina nanoparticles is discussed by Khan et al. [20]. Coriolis force effects on the dynamics of an MHD rotating fluid are presented by Lou et al. [21]. The hyperbolic nanofluid flow of irregular thickness across a slender elastic surface is presented by Ashraf et al. [22]. The Lorentz and buoyancy forces' importance on bioconvection flow dynamics is discussed by Ali et al. [23]. Furthermore, a few related studies using the mass/heat transfer are discussed in Refs. [24–26].

The current study represents the numerical performances of the Williamson nanofluid model (WNM) using the novel hyperbolic tangent sigmoid function. These investigations of the WNF model by using the designated stochastic procedure have never been implemented. In this study, the idea to exploit the hyperbolic tangent sigmoid function is presented for the first time to solve the WNM. The WNM is classified into two velocities, concentration and temperature. A targeted dataset through the Adam scheme is achieved that is further accomplished using the procedure of training, testing, and verification with ratios 0.15, 0.13, and 0.72. Fifteen and thirty neurons have been used in layer one and two. Recently, the stochastic process using the neural networks were explored in several submissions, e.g., the dengue fever model [27], the thermal explosion theory [28], the food chain model [29], and the HIV model [30]. Some novel topographies of current research are itemized as:

1. A learning deep neural network process is presented for the first time for the numerical solutions of the WNF system.
2. A process of deep neural network using the amounts of fifteen and thirty neurons is presented for solving the model.
3. The hyperbolic tangent sigmoid transfer function is used in the hidden layers.
4. A Bayesian regularization for the optimization procedure is presented for solving the WNF system.
5. A targeted dataset through the Adam scheme is achieved that is further accomplished based on training, testing, and verification with ratios of 0.15, 0.13, and 0.72.
6. The accuracy of the scheme is pragmatic through the comparison of the solutions, whereas the negligible absolute error (AE) enhances the correctness of the technique.

The fluid model is presented into three classes, dimensionless stream, concentration, and temperature [31], while the parameter performances for the WNF are given in Table 1. The mathematical form of the WNF is shown as:

$$\begin{cases} \left(\lambda_1 \frac{d^2 f}{dv^2} + 1\right)\frac{d^3 f}{dv^3} - \frac{df}{dv}\left(\frac{df}{dv} + M\sin^2\rho\right) = 0, \\ \frac{1}{\Pr}\frac{d^2\theta}{dv^2} + f\frac{d\theta}{dv} + Nt\left(\frac{d\theta}{dv}\right)^2 + Nb\frac{d\theta}{dv}\frac{d\phi}{dv} = 0, \\ \frac{d^2\phi}{dv^2} + \frac{Nt}{Nb}\frac{d^2\theta}{dv^2} + Le\left(f\frac{d\phi}{dv}\right) = 0. \end{cases} \tag{1}$$

The boundary conditions (BCs) of the above model are given as [29–34]:

$$f(0) = 0,\ \phi(0) = 1,\ \frac{d\theta(0)}{du} = -Bi(1-\theta(0)),\ \ \frac{df(1)}{du} = 0,\ \frac{df(0)}{du} = 1,\ \theta(1) = 0,\ \text{and}\ \phi(1) = 0.$$

Table 1. Parameter performances for the WNF.

Parameters	Description
Nt	Thermophoresis parameter
M	Magnetic parameter
Bi	Biot number
ρ	Inclination angle
λ_1	Williamson parameter
Le	Lewis number
Pr	Prandtl number
Nb	Parameter of Brownian motion
v	Input

The remaining sections are presented as follows. The deep neural network procedure for the WNF system is shown in Section 2. Detailed results of the model using the stochastic procedure are presented in Section 3, while the conclusions are reported in Section 4.

2. Methodology

The deep neural networking for solving the fluid model is presented with the necessary deep neural network process along with the execution performances.

2.1. Deep Neural Network Process

The current section presents the layers structure based on the amounts of fifteen and thirteen neurons in layers 1 and 2. A transfer hyperbolic tangent sigmoid function is applied as an activation function to solve the WNF model. A three-layer structure with a feed-forward neural network is mathematically shown as:

$$\begin{bmatrix} u_1 \\ u_2 \\ u_3 \\ . \\ . \\ . \\ u_{15} \end{bmatrix} = \triangle \left(\begin{bmatrix} w_{1,1} \\ w_{1,2} \\ w_{1,3} \\ . \\ . \\ . \\ w_{1,15} \end{bmatrix} [v] + \begin{bmatrix} b_{1,1} \\ b_{1,2} \\ b_{1,3} \\ . \\ . \\ . \\ b_{1,15} \end{bmatrix} \right), \tag{2}$$

$$\begin{bmatrix} s_1 \\ s_2 \\ s_3 \\ . \\ . \\ . \\ s_{30} \end{bmatrix} = \delta \left(\begin{bmatrix} \psi_{1,1} & \psi_{2,1} & \psi_{3,1} & . & . & . & \psi_{15,1} \\ \psi_{1,2} & \psi_{2,2} & \psi_{3,2} & . & . & . & \psi_{15,2} \\ \psi_{1,3} & \psi_{2,3} & \psi_{3,3} & . & . & . & \psi_{15,3} \\ . & . & . & . & . & . & . \\ . & . & . & . & . & . & . \\ . & . & . & . & . & . & . \\ \psi_{1,30} & \psi_{2,30} & \psi_{3,30} & . & . & . & \psi_{15,30} \end{bmatrix} \begin{bmatrix} u_1 \\ u_2 \\ u_3 \\ . \\ . \\ . \\ u_{15} \end{bmatrix} + \begin{bmatrix} b_{2,1} \\ b_{2,2} \\ b_{2,3} \\ . \\ . \\ . \\ b_{2,30} \end{bmatrix} \right), \tag{3}$$

$$\begin{bmatrix} f(v) \\ \theta(v) \\ \phi(v) \end{bmatrix} = \Delta \left(\begin{bmatrix} \omega_{1,1} & \omega_{2,1} & \omega_{3,1} & . & . & . & \omega_{30,1} \\ \omega_{1,2} & \omega_{2,2} & \omega_{3,2} & . & . & . & \omega_{30,2} \\ \omega_{1,3} & \omega_{2,3} & \omega_{3,3} & . & . & . & \omega_{30,3} \end{bmatrix} \begin{bmatrix} s_1 \\ s_2 \\ s_3 \\ . \\ . \\ . \\ s_{30} \end{bmatrix} + \begin{bmatrix} b_{3,1} \\ b_{3,2} \\ b_{3,3} \end{bmatrix} \right). \tag{4}$$

In the above equations, w, ψ and ω represent the first, second, and output layer weights, respectively; b is neuron bias, u and s are the first- and second-layer outputs,

$f(v)$, $\theta(v)$ and $\phi(v)$ are the obtained outputs, and Δ is the activation function based on the hyperbolic tangent sigmoid function, given as:

$$\Delta = \frac{2}{1+e^{(-2q)}} - 1, \text{ where } q = \sum_{i=1}^{m}(w_i s_i) + b, \tag{5}$$

The numbers of neurons are represented by m. Figure 1 shows the three-step structure, mathematical system, multi-layer neural network, and achieved performances for solving the WNF system. A targeted dataset through the Adam scheme is achieved that is further accomplished using the training, testing, and verification by taking 0.15, 0.13, and 0.72. Figure 2 shows the neural network multi-layer process for solving the WNF system using the deep neural network procedure. In this figure, in the hidden layers 1 and 2, fifteen and twenty neurons have been used, while three outputs have been presented.

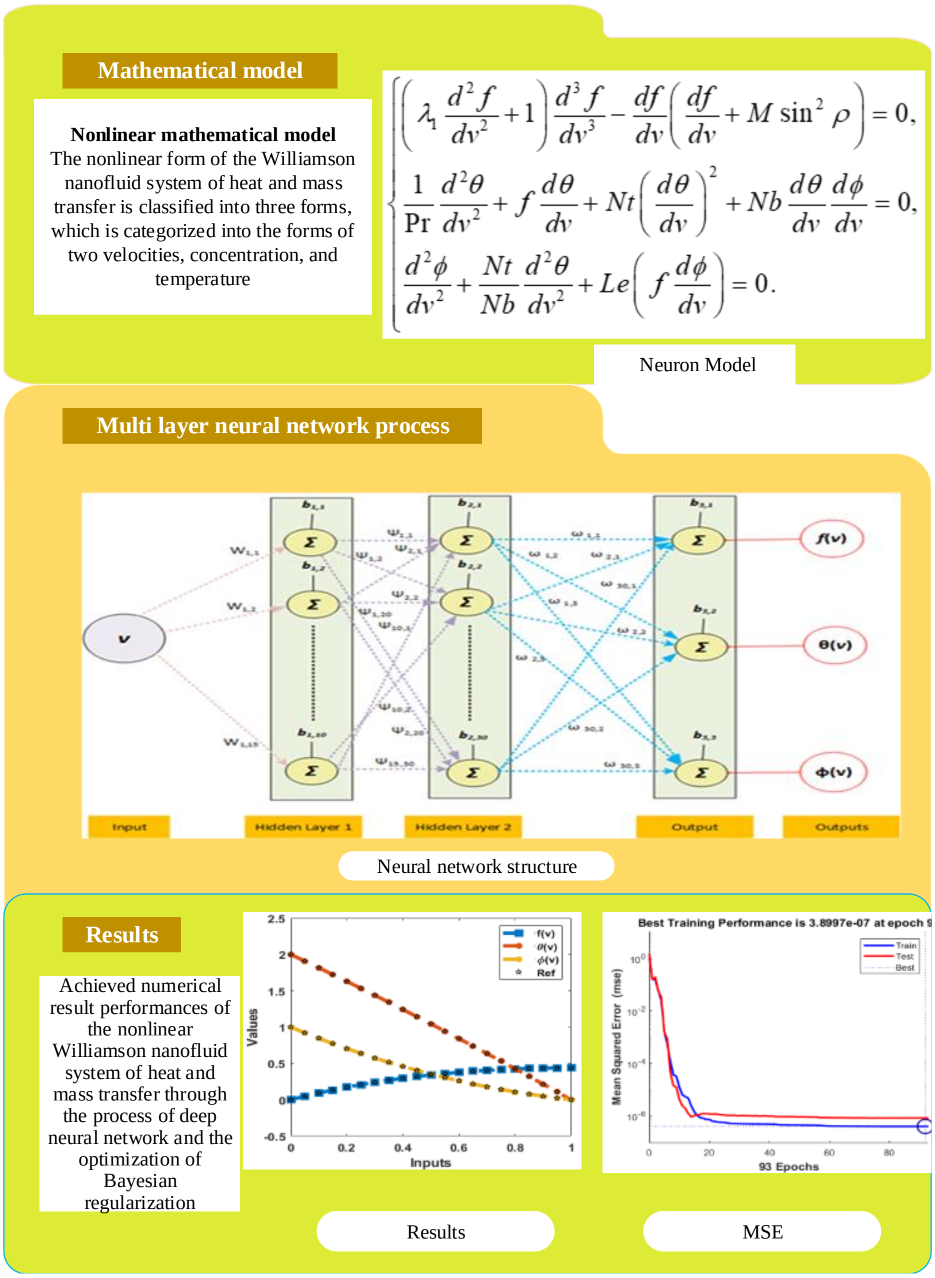

$$\begin{cases} \left(\lambda_1 \frac{d^2 f}{dv^2} + 1\right)\frac{d^3 f}{dv^3} - \frac{df}{dv}\left(\frac{df}{dv} + M\sin^2\rho\right) = 0, \\ \frac{1}{\Pr}\frac{d^2\theta}{dv^2} + f\frac{d\theta}{dv} + Nt\left(\frac{d\theta}{dv}\right)^2 + Nb\frac{d\theta}{dv}\frac{d\phi}{dv} = 0, \\ \frac{d^2\phi}{dv^2} + \frac{Nt}{Nb}\frac{d^2\theta}{dv^2} + Le\left(f\frac{d\phi}{dv}\right) = 0. \end{cases}$$

Figure 1. Proposed mathematical system, multi-layer performances and achieved results for WNF system.

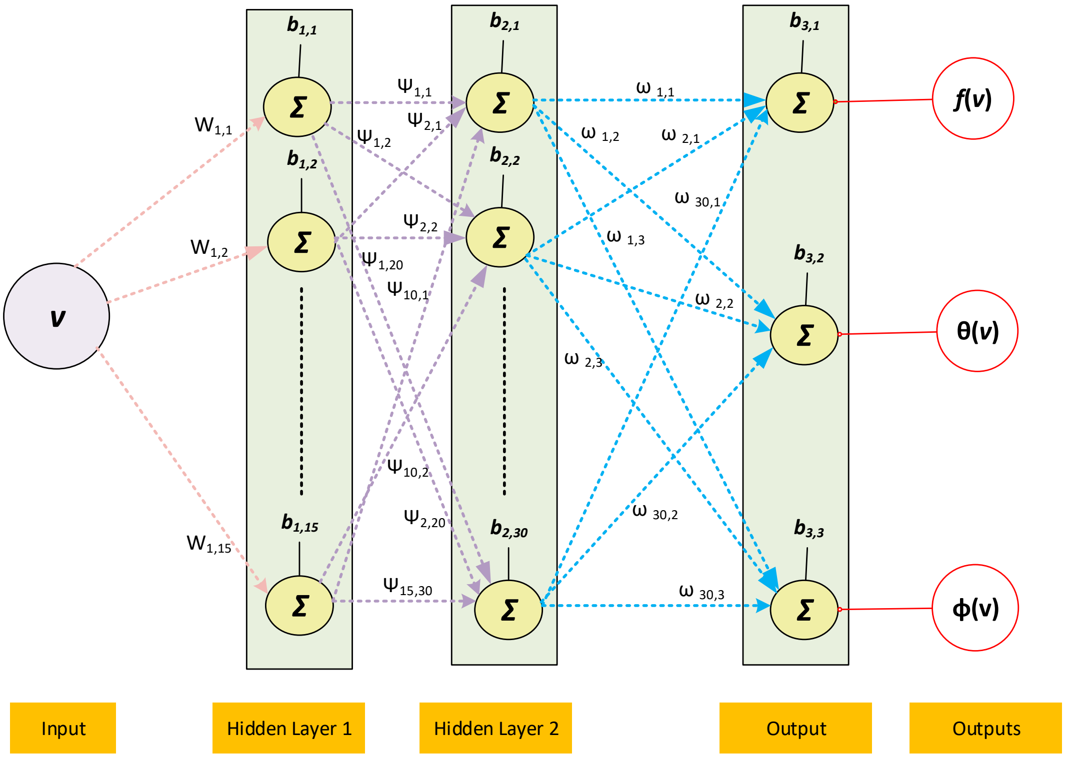

Figure 2. Multilayer procedure for solving the WNF using the deep neural network.

Figure 3 shows the deep neural network and hidden layer structure for solving the WNF system. Figure 3a shows the layer structure based on a single input, hidden layers, and the hyperbolic tangent sigmoid function with 3 outputs. This figure is performed on the basis of case 1 of the model, which shows that the maximum 750 Epochs have been used; time, performance, Mu values, and gradient are also presented. Figure 3b represents the layers' structure for solving the WNF nonlinear model. The input, two hidden and output layers, has been presented in this figure. *W* shows the weight vectors, *b* is the bias, and three outputs have been illustrated.

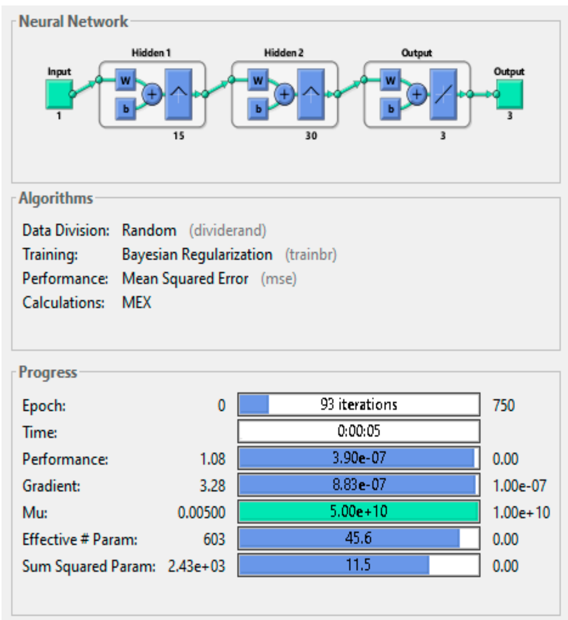

(**a**)

Figure 3. *Cont.*

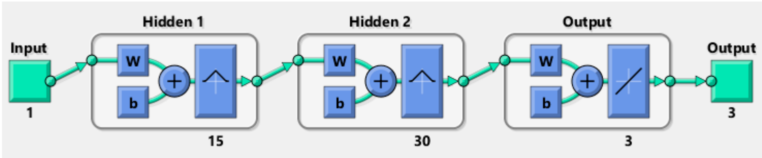

(**b**)

Figure 3. Neural network and hidden layers' structure for the WNF system. (**a**) Neural network structure for the WNF system. (**b**) Hidden layer structure.

2.2. Bayesian Regularization (BR)

Bayesian regularization (BR) is considered one of the robust and efficient back-propagation net procedures, which is used to reduce or eliminate the lengthy process through cross-validation. BR represents the mathematical performances, which shift a nonlinear regression process into a unique statistical model based on ridge regression. BR provides the numerical performances of various modeling, e.g., robustness, model choice, authentication size, and optimization of net construction.

3. Simulations and Results

The current section shows the detailed results for three cases of the WNF system using the process of a deep neural network, mathematically given as:

Case 1: Consider $\mathrm{Pr} = \frac{1}{5}$, $M = \frac{1}{2}$, $\rho = \frac{\pi}{6}$, $\lambda_1 = \frac{1}{5}$, $Le = 1$, $Nb = \frac{1}{5}$, $Bi = \frac{1}{2}$, and $Nt = \frac{1}{2}$, given as:

$$\begin{cases} \left(\frac{1}{5}\frac{d^2 f}{dv^2} + 1\right)\frac{d^3 f}{dv^3} - \frac{df}{dv}\left(\frac{df}{dv} + \frac{1}{2}\sin^2\frac{\pi}{6}\right) = 0, \\ 5\frac{d^2\theta}{dv^2} + \frac{1}{2}\left(\frac{d\theta}{dv}\right)^2 + f\frac{d\theta}{dv} + \frac{1}{5}\frac{d\phi}{dv}\frac{d\theta}{dv} = 0, \\ \frac{d^2\phi}{dv^2} + \left(f\frac{d\phi}{dv}\right) + \frac{5}{2}\frac{d^2\theta}{dv^2} = 0. \end{cases} \tag{6}$$

Case 2: Consider $\mathrm{Pr} = 2$, $M = \frac{1}{2}$, $\rho = \frac{\pi}{6}$, $\lambda_1 = \frac{1}{5}$, $Le = 1$, $Nb = \frac{1}{5}$, $Bi = \frac{1}{2}$, and $Nt = \frac{1}{2}$, given as:

$$\begin{cases} \left(\frac{1}{5}\frac{d^2 f}{dv^2} + 1\right)\frac{d^3 f}{dv^3} - \frac{df}{dv}\left(\frac{df}{dv} + \frac{1}{2}\sin^2\frac{\pi}{6}\right) = 0, \\ \frac{1}{2}\frac{d^2\theta}{dv^2} + \frac{1}{2}\left(\frac{d\theta}{dv}\right)^2 + f\frac{d\theta}{dv} + \frac{1}{5}\frac{d\phi}{dv}\frac{d\theta}{dv} = 0, \\ \frac{d^2\phi}{dv^2} + \left(f\frac{d\phi}{dv}\right) + \frac{5}{2}\frac{d^2\theta}{dv^2} = 0. \end{cases} \tag{7}$$

Case 3: $\mathrm{Pr} = 7$, $M = \frac{1}{2}$, $\rho = \frac{\pi}{6}$, $\lambda_1 = \frac{1}{5}$, $Le = 1$, $Nb = \frac{1}{5}$, $Bi = \frac{1}{2}$, and $Nt = \frac{1}{2}$, given as:

$$\begin{cases} \left(\frac{1}{5}\frac{d^2 f}{dv^2} + 1\right)\frac{d^3 f}{dv^3} - \frac{df}{dv}\left(\frac{df}{dv} + \frac{1}{2}\sin^2\frac{\pi}{6}\right) = 0, \\ \frac{1}{7}\frac{d^2\theta}{dv^2} + \frac{1}{2}\left(\frac{d\theta}{dv}\right)^2 + f\frac{d\theta}{dv} + \frac{1}{5}\frac{d\phi}{dv}\frac{d\theta}{dv} = 0, \\ \frac{d^2\phi}{dv^2} + \left(f\frac{d\phi}{dv}\right) + \frac{5}{2}\frac{d^2\theta}{dv^2} = 0. \end{cases} \tag{8}$$

The BCs of each case are $f(0) = 0$, $\frac{df(0)}{du} = 1$, $\frac{d\theta(0)}{du} = -\frac{1}{2}(1 - \theta(0))$, $\frac{df(1)}{du} = 0$, $\phi(0) = 1$, $\theta(1) = 0$ and $\phi(1) = 0$.

A process of a deep neural network with the hyperbolic tangent sigmoid transfer function along with the optimization of BR is given for the numerical treatment of the nonlinear model. The input values are selected as [0, 1], while the step size is 0.01. A tangent hyperbolic sigmoid transfer function is used in both hidden layers with fifteen and thirty neurons for solving the model. Figure 4 shows the transition of state (ToS) and mean square error (MSE) using the nonlinear model. The maximum number of epochs has been taken as 750. Figure 4 shows the MSE performances, which are calculated as $8.8997 \times 10^{-0.7}$, $1.0091 \times 10^{-0.63}$, and $1.1656 \times 10^{-0.6}$ at epochs 93, 203, and 224. Figure 4 signifies the gradient measures, Mu values, sum squared performances, num parameter, and authentication checks. The gradient measures are illustrated in Figure 4, which are given as $8.827 \times 10^{-0.7}$, $1.7593 \times 10^{-0.6}$, and $5.3555 \times 10^{-0.5}$.

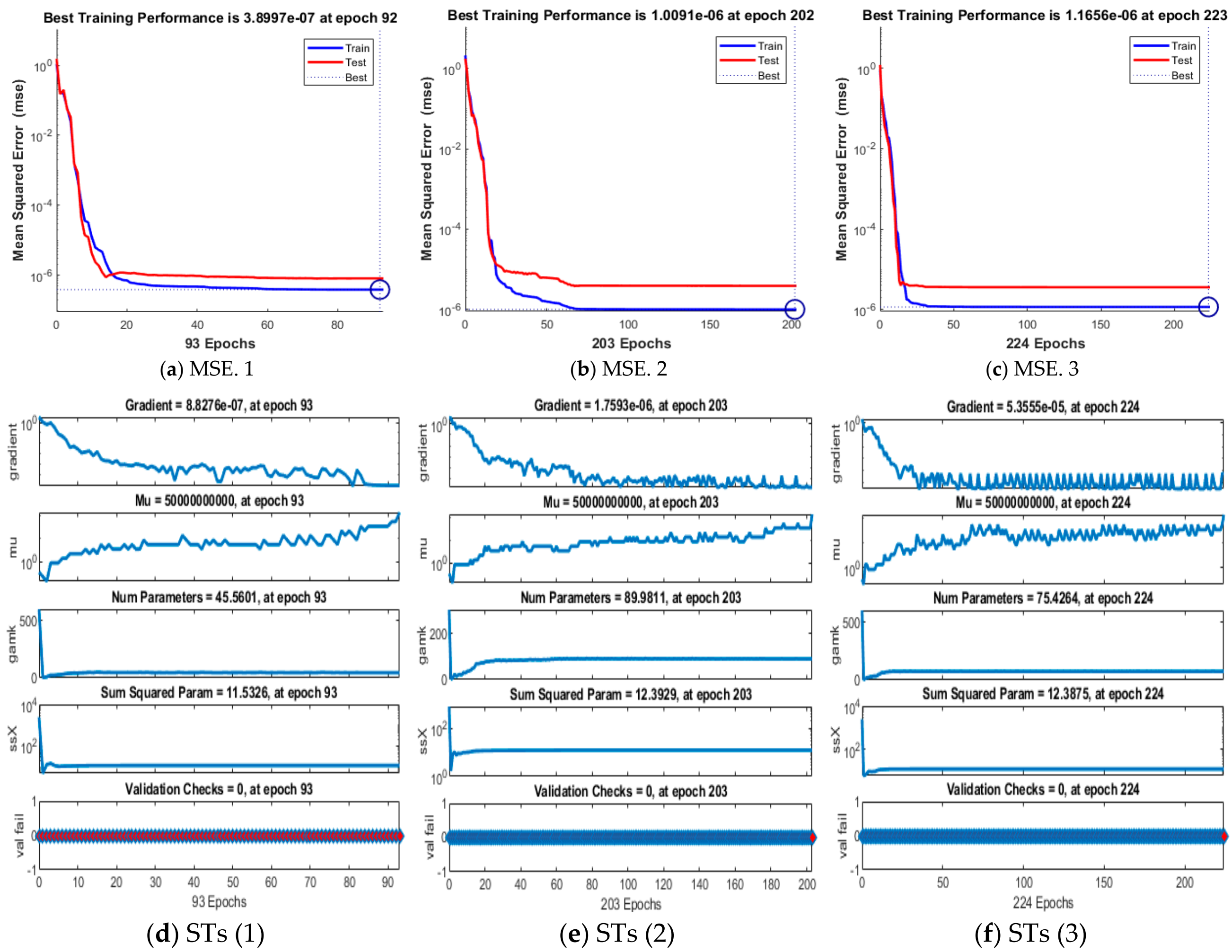

Figure 4. Illustrations of the best training and STs' (gradient, Mu, epochs, num parameters) performances to solve the nonlinear WNF system.

Figures 5–7 are the function fitness (Func. Fit) for solving the nonlinear model using the process of a deep neural network transfer function hyperbolic tangent sigmoid by using the optimization procedures of BR. Figure 8 authenticates the values of the error histograms (EHs) for solving the model and these values are calculated as $-1.60 \times 10^{-0.5}$, $4.10 \times 10^{-0.4}$, and $-8.30 \times 10^{-0.7}$. The performances of regression (Reg) for cases 1 to 3 are authenticated in Figure 9 to solve the model using the process of a deep neural network, which are found as 1 (perfect modelling). MSE values of train/test statics are presented in Table 2 for solving the nonlinear model.

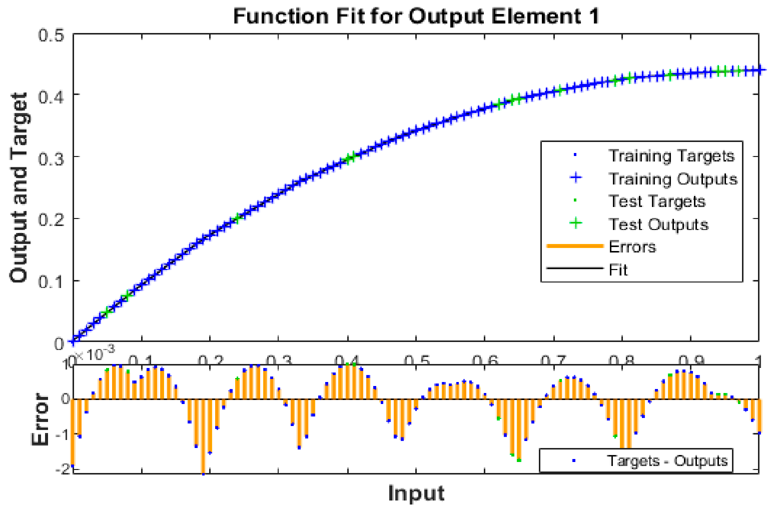

Figure 5. Func. Fit for the nonlinear WNF model (1).

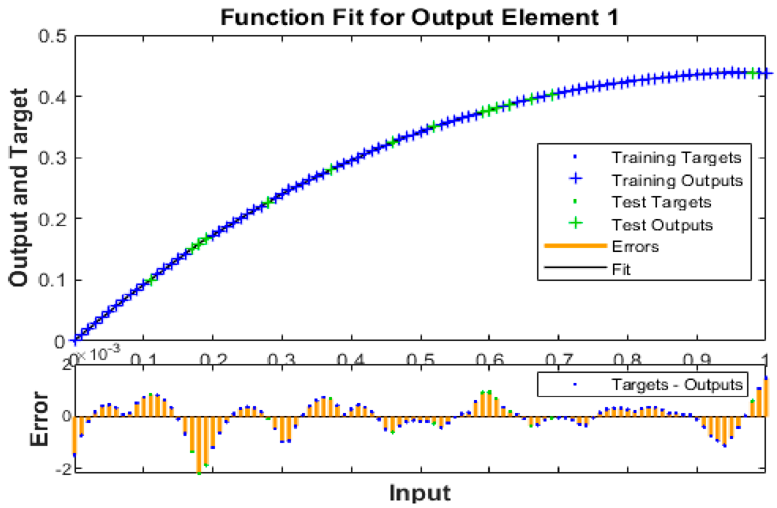

Figure 6. Func. Fit for the nonlinear WNF model (2).

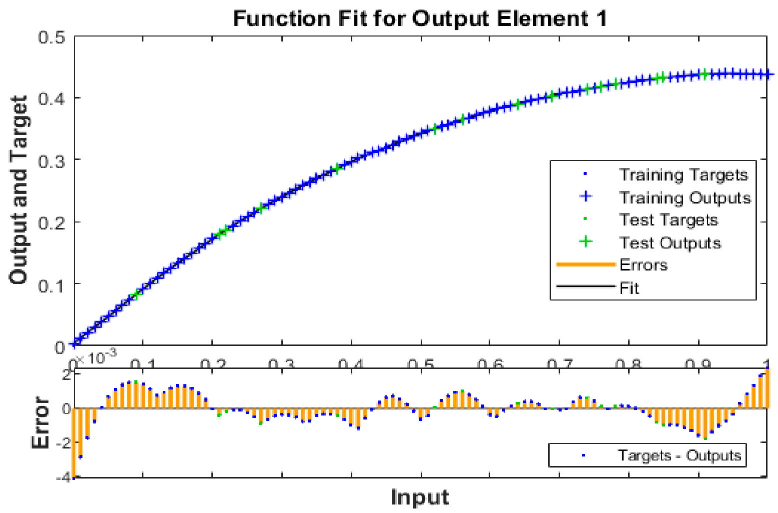

Figure 7. Func. Fit for the nonlinear WNF model (3).

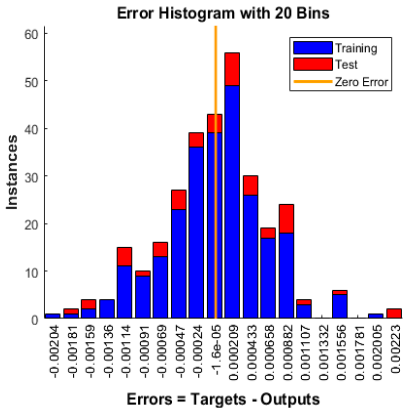

(**a**) EHs of case 1

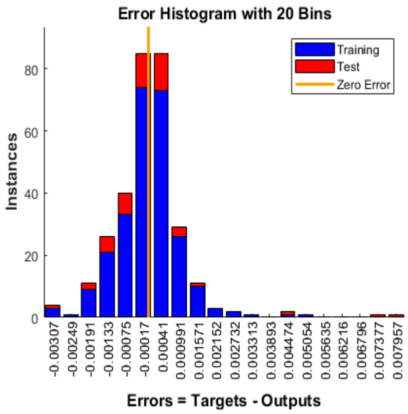

(**b**) EHs of case 2

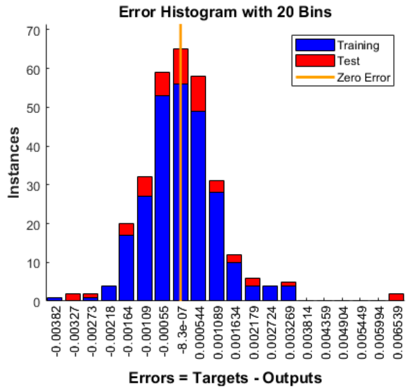

(**c**) EHs of case 3

Figure 8. EHs for the nonlinear WNF model 1 to 3.

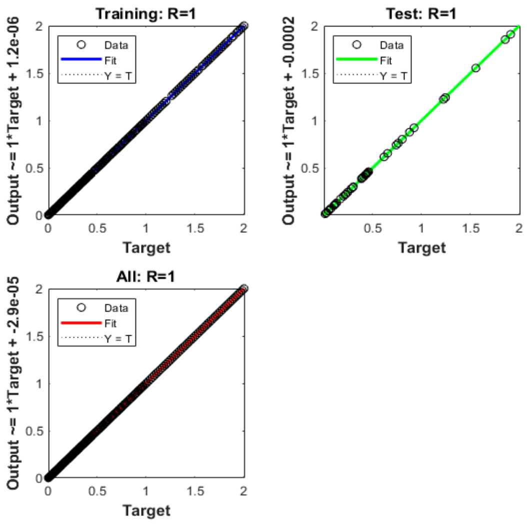

(**a**) Reg. (1)

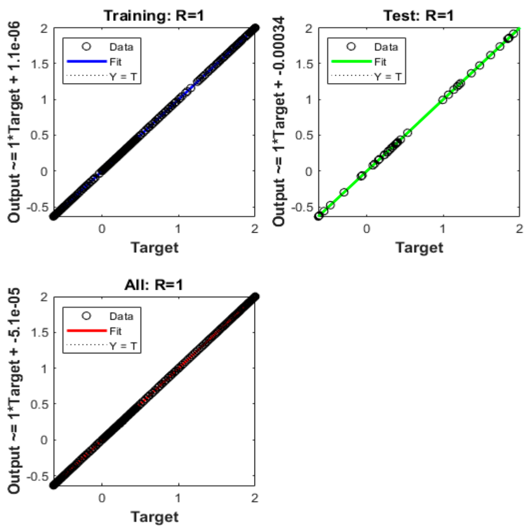

(**b**) Reg. (2)

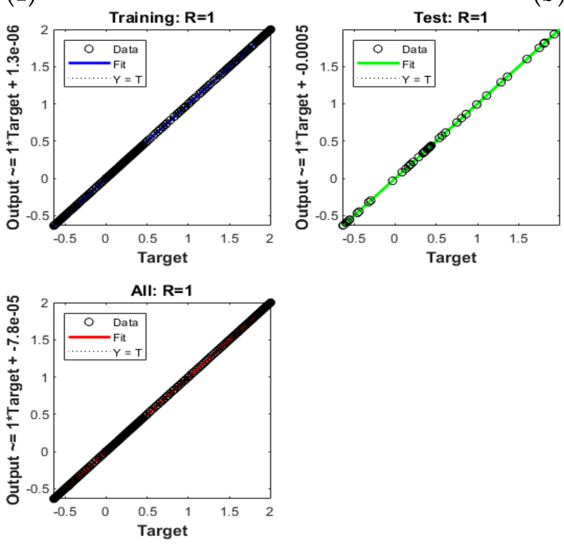

(**c**) Reg. (3)

Figure 9. Regression measures for nonlinear WNF model 1 to 3.

Table 2. Proposed scheme for solving the nonlinear fluid model.

Case	MSE		Performance	Gradient	Epoch	Time
	Test	Train				
1	$8.1633 \times 10^{-0.7}$	$3.8997 \times 10^{-0.7}$	$3.90 \times 10^{-0.7}$	$8.83 \times 10^{-0.7}$	93	5 s
2	$1.0091 \times 10^{-0.6}$	$3.8968 \times 10^{-0.6}$	$1.01 \times 10^{-0.6}$	$1.76 \times 10^{-0.6}$	203	2 s
3	$1.1656 \times 10^{-0.6}$	$3.6107 \times 10^{-0.6}$	$1.17 \times 10^{-0.6}$	$5.36 \times 10^{-0.5}$	224	12 s

Figure 10 represents the results' comparisons of outputs $f(v)$, $\theta(v)$ and $\phi(v)$. The results matching show the performances of the outcomes for each category of the nonlinear fluid model, which shows the exactness of the nonlinear model.

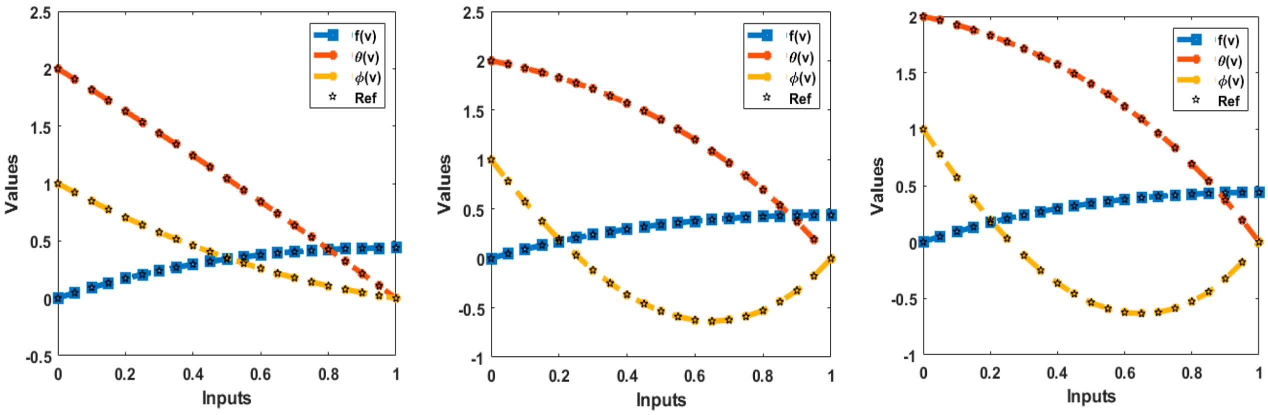

(**a**) Results comparison (1) (**b**) Results comparison (2) (**c**) Results comparison (3)

Figure 10. Comparisons of the results for the nonlinear WNF model 1 to 3.

The values of AE using the performances $f(v)$, $\theta(v)$ and $\phi(v)$ are shown in Table 3 for the numerical solutions of the nonlinear WNF model 1 to 3. These performances have been reported by taking the 0.1 step size in input 0 and 1. The negligible values of AE for the parameters $f(v)$, $\theta(v)$ and $\phi(v)$ are calculated around 10^{-04} to 10^{-07} for each class of the model that represents the correctness of the scheme.

Table 3. AE for the parameters $f(v)$, $\theta(v)$ and $\phi(v)$ of the model.

v	0	0.1	0.2	0.3	0.4	0.5	0.6	0.7	0.8	0.9	1
$f(v)$	2×10^{-3}	6×10^{-4}	2×10^{-3}	3×10^{-4}	1×10^{-3}	3×10^{-4}	1×10^{-4}	4×10^{-4}	2×10^{-3}	8×10^{-4}	1×10^{-3}
	1×10^{-3}	7×10^{-4}	1×10^{-3}	1×10^{-3}	3×10^{-4}	2×10^{-4}	9×10^{-4}	5×10^{-5}	3×10^{-4}	1×10^{-4}	1×10^{-3}
	4×10^{-3}	1×10^{-3}	7×10^{-6}	4×10^{-4}	1×10^{-3}	6×10^{-4}	4×10^{-4}	8×10^{-5}	1×10^{-4}	2×10^{-3}	2×10^{-3}
$\theta(v)$	2×10^{-4}	3×10^{-4}	4×10^{-4}	8×10^{-5}	4×10^{-4}	7×10^{-5}	2×10^{-5}	2×10^{-4}	7×10^{-4}	3×10^{-4}	4×10^{-4}
	2×10^{-4}	4×10^{-5}	2×10^{-3}	2×10^{-3}	8×10^{-4}	2×10^{-3}	9×10^{-4}	2×10^{-4}	1×10^{-3}	1×10^{-3}	1×10^{-3}
	1×10^{-3}	3×10^{-4}	8×10^{-4}	2×10^{-4}	4×10^{-4}	8×10^{-4}	3×10^{-4}	4×10^{-4}	6×10^{-4}	1×10^{-3}	2×10^{-3}
$\phi(v)$	6×10^{-4}	5×10^{-4}	7×10^{-4}	2×10^{-4}	1×10^{-3}	2×10^{-4}	2×10^{-6}	7×10^{-4}	2×10^{-3}	1×10^{-4}	3×10^{-4}
	2×10^{-3}	8×10^{-4}	5×10^{-3}	5×10^{-3}	2×10^{-3}	1×10^{-3}	2×10^{-4}	1×10^{-3}	5×10^{-4}	7×10^{-4}	2×10^{-4}
	3×10^{-3}	4×10^{-4}	2×10^{-3}	1×10^{-3}	2×10^{-3}	3×10^{-3}	2×10^{-3}	2×10^{-4}	2×10^{-3}	5×10^{-4}	3×10^{-3}

4. Concluding Remarks

The current study shows the design of the novel hyperbolic tangent sigmoid function for the numerical treatment of the Williamson nanofluid model (WNM), which is classified into two velocities, concentration and temperature. Some of the concluding remarks of this work are as follows.

A deep neural network procedure using fifteen and thirty neurons is presented through the hyperbolic tangent sigmoid transfer function in the hidden layers.

1. The optimization is performed through the Bayesian regularization, while the hyperbolic tangent sigmoid transfer function in the hidden layers is used.
2. The numerical performances of the results have been proposed using the stochastic computing schemes along with the process of a deep neural network and Bayesian regularization.
3. A targeted dataset 'Adam' scheme is designed, which is further accomplished based on the procedure of training, testing, and verification using the ratios of 0.15, 0.13, and 0.72.
4. The correctness of the deep neural network along with BRA has been performed through the overlapping of the solutions and small absolute error.
5. The capability of the procedure using the statistical observations is authenticated to reduce the mean square error for the nonlinear WNM.

In future, the designed novel deep neural network along with BRA can be executed to present the numerical solutions of various dynamical models [32–34].

Author Contributions: Methodology, B.S.; Software, Z.S.; Formal analysis, B.S. All authors have read and agreed to the published version of the manuscript.

Funding: This work was supported by the Deanship of Scientific Research, Vice Presidency for Graduate Studies and Scientific Research, King Faisal University, Saudi Arabia (Grant No. 2376).

Data Availability Statement: The data that support the findings of this study are available from the corresponding author upon reasonable request.

Acknowledgments: The authors are very grateful for the support of Scientific Research, Vice Presidency for Graduate Studies and Scientific Research, King Faisal University, Saudi Arabia (Grant No. 2376).

Conflicts of Interest: The authors declare no conflict of interest.

References

1. Bhatti, M.M.; Rashidi, M.M. Entropy generation with nonlinear thermal radiation in MHD boundary layer flow over a permeable shrinking/stretching sheet: Numerical solution. *J. Nanofluids* **2016**, *5*, 543–548. [CrossRef]
2. Alharbi, K.A.M.; Yasmin, S.; Farooq, S.; Waqas, H.; Alwetaishi, M.; Khan, S.U.; Al-Turjman, F.; Elattar, S.; Khan, M.I.; Galal, A.M. Thermal outcomes of Williamson pseudo-plastic nanofluid with microorganisms due to the heated Riga surface with bio-fuel applications. *Waves Random Complex Media* **2022**, 1–24. [CrossRef]
3. Texter, J.; Qiu, Z.; Crombez, R.; Byrom, J.; Shen, W. Nanofluid acrylate composite resins—Initial preparation and characterization. *Polym. Chem.* **2011**, *2*, 1778–1788. [CrossRef]
4. Krishnamurthy, M.; Prasannakumara, B.; Gireesha, B.; Gorla, R.S.R. Effect of chemical reaction on MHD boundary layer flow and melting heat transfer of Williamson nanofluid in porous medium. *Eng. Sci. Technol. Int. J.* **2016**, *19*, 53–61. [CrossRef]
5. Hayat, T.; Anum Shafiq, A. Alsaedi, Hydromagnetic Boundary Layer Flow of Williamson Fluid in the Presence of Thermal Radiation and Ohmic Dissipation. *Alex. Eng. J.* **2016**, *55*, 2229–2240. [CrossRef]
6. Bordag, M. Drude model and Lifshitz formula. *Eur. Phys. J. C* **2011**, *71*, 1788. [CrossRef]
7. Bhatti, M.M.; Abbas, T.; Rashidi, M.M. Effects of thermal radiation and electromagnetohydrodynamics on viscous nanofluid through a Riga plate. *Multidiscip. Model. Mater. Struct.* **2016**, *12*, 605–618. [CrossRef]
8. Goud, B.S.; Madhu, J.V.; Shekar, M.R. MHD Viscous Dissipative Fluid Flows In a Channel with a Stretching and Porous Plate with Radiation Effect. *Int. J. Innov. Technol. Explor. Eng.* **2019**, *8*, 1877–1882. [CrossRef]
9. Kumar, P.P.; Goud, B.S.; Malga, B.S. Finite element study of Soret number effects on MHD flow of Jeffrey fluid through a vertical permeable moving plate. *Partial. Differ. Equ. Appl. Math.* **2020**, *1*, 100005. [CrossRef]
10. Sreenadh, S.; Govardhan, P.; Kumar, Y.R. Effects of slip and heat transfer on the peristaltic pumping of a Williamson fluid in an inclined channel. *Int. J. Appl. Sci. Eng.* **2014**, *12*, 143–155.
11. Rao, J.S.S.; Prasad, R.S.; Dharmavaram, A.D. Free Convective Fully Developed Flow of A Williamson Fluid in A Vertical Channel with An Effect of Inclined Magnetic Feild. *J. Comput. Math. Sci.* **2014**, *5*, 412–481.
12. Ayub, A.; Sabir, Z.; Le, D.-N.; Aly, A.A. Nanoscale heat and mass transport of magnetized 3-D chemically radiative hybrid nanofluid with orthogonal/inclined magnetic field along rotating sheet. *Case Stud. Therm. Eng.* **2021**, *26*, 101193. [CrossRef]

13. Ayub, A.; Wahab, H.A.; Shah, S.Z.; Shah, S.L.; Darvesh, A.; Haider, A.; Sabir, Z. Interpretation of infinite shear rate viscosity and a nonuniform heat sink/source on a 3D radiative cross nanofluid with buoyancy assisting/opposing flow. *Heat Transf.* **2021**, *50*, 4192–4232. [CrossRef]
14. Nadeem, S.; Hussain, S.T. Flow and heat transfer analysis of Williamson nanofluid. *Appl. Nanosci.* **2013**, *4*, 1005–1012. [CrossRef]
15. Venkataramanaiah, G.; Sreedharbabu, M.; Lavanya, M. Heat generation/absorption effects on magneto-williamson nanofluidflow with heat and mass fluxes. *Int. J. Eng. Dev. Res.* **2016**, *4*, 384–398.
16. Hussanan, A.; Salleh, M.Z.; Khan, I. Microstructure and inertial characteristics of a magnetite ferrofluid over a stretching/shrinking sheet using effective thermal conductivity model. *J. Mol. Liq.* **2018**, *255*, 64–75. [CrossRef]
17. Hussanan, A.; Qasim, M.; Chen, Z.-M. Heat transfer enhancement in sodium alginate based magnetic and non-magnetic nanoparticles mixture hybrid nanofluid. *Phys. A Stat. Mech. Appl.* **2020**, *550*, 123957. [CrossRef]
18. Qureshi, M.Z.A.; Faisal, M.; Raza, Q.; Ali, B.; Botmart, T.; Shah, N.A.; Qureshi, M.Z.A.; Faisal, M.; Raza, Q.; Ali, B. Morphological nanolayer impact on hybrid nanofluids flow due to dispersion of polymer/CNT matrix nanocomposite material. *AIMS Math.* **2023**, *8*, 633–656. [CrossRef]
19. Raza, Q.; Qureshi, M.Z.A.; Khan, B.A.; Hussein, A.K.; Ali, B.; Shah, N.A.; Chung, J.D. Insight into Dynamic of Mono and Hybrid Nanofluids Subject to Binary Chemical Reaction, Activation Energy, and Magnetic Field through the Porous Surfaces. *Mathematics* **2022**, *10*, 3013. [CrossRef]
20. Khan, S.A.; Eze, C.; Lau, K.T.; Ali, B.; Ahmad, S.; Ni, S.; Zhao, J. Study on the novel suppression of heat transfer deterioration of supercritical water flowing in vertical tube through the suspension of alumina nanoparticles. *Int. Commun. Heat Mass Transf.* **2022**, *132*, 105893. [CrossRef]
21. Lou, Q.; Ali, B.; Rehman, S.U.; Habib, D.; Abdal, S.; Shah, N.A.; Chung, J.D. Micropolar Dusty Fluid: Coriolis Force Effects on Dynamics of MHD Rotating Fluid When Lorentz Force Is Significant. *Mathematics* **2022**, *10*, 2630. [CrossRef]
22. Ashraf, M.Z.; Rehman, S.U.; Farid, S.; Hussein, A.K.; Ali, B.; Shah, N.A.; Weera, W. Insight into Significance of Bioconvection on MHD Tangent Hyperbolic Nanofluid Flow of Irregular Thickness across a Slender Elastic Surface. *Mathematics* **2022**, *10*, 2592. [CrossRef]
23. Ali, B.; Ali, M.; Saman, I.; Hussain, S.; Yahya, A.U.; Hussain, I. Tangent hyperbolic nanofluid: Significance of Lorentz and buoyancy forces on dynamics of bioconvection flow of rotating sphere via finite element simulation. *Chin. J. Phys.* **2022**, *77*, 658–671. [CrossRef]
24. Ali, B.; Khan, S.A.; Hussein, A.K.; Thumma, T.; Hussain, S. Hybrid nanofluids: Significance of gravity modulation, heat source/ sink, and magnetohydrodynamic on dynamics of micropolar fluid over an inclined surface via finite element simulation. *Appl. Math. Comput.* **2021**, *419*, 126878. [CrossRef]
25. Kho, Y.B.; Hussanan, A.; Mohamed, M.K.A.; Salleh, M.Z. Heat and mass transfer analysis on flow of Williamson nanofluid with thermal and velocity slips: Buongiorno model. *Propuls. Power Res.* **2019**, *8*, 243–252. [CrossRef]
26. Shah, S.Z.H.; Wahab, H.A.; Ayub, A.; Sabir, Z.; Haider, A.; Shah, S.L. Higher order chemical process with heat transport of magnetized cross nanofluid over wedge geometry. *Heat Transf.* **2021**, *50*, 3196–3219. [CrossRef]
27. Umar, M.; Sabir, Z.; Raja, M.A.Z.; Sánchez, Y.G. A stochastic numerical computing heuristic of SIR nonlinear model based on dengue fever. *Results Phys.* **2020**, *19*, 103585. [CrossRef]
28. Sabir, Z. Neuron analysis through the swarming procedures for the singular two-point boundary value problems arising in the theory of thermal explosion. *Eur. Phys. J. Plus* **2022**, *137*, 638. [CrossRef]
29. Sabir, Z. Stochastic numerical investigations for nonlinear three-species food chain system. *Int. J. Biomath.* **2022**, *15*, 2250005. [CrossRef]
30. Umar, M.; Sabir, Z.; Raja, M.A.Z.; Baskonus, H.M.; Yao, S.-W.; Ilhan, E. A novel study of Morlet neural networks to solve the nonlinear HIV infection system of latently infected cells. *Results Phys.* **2021**, *25*, 104235. [CrossRef]
31. Srinivasulu, T.; Goud, B.S. Effect of inclined magnetic field on flow, heat and mass transfer of Williamson nanofluid over a stretching sheet. *Case Stud. Therm. Eng.* **2021**, *23*, 100819. [CrossRef]
32. Ilhan, E.; Kıymaz, I.O. A generalization of truncated M-fractional derivative and applications to fractional differential equations. *Appl. Math. Nonlinear Sci.* **2020**, *5*, 171–188. [CrossRef]
33. Ammar, M.K.; Amin, M.R.; Hassan, M. Visibility intervals between two artificial satellites under the action of Earth oblateness. *Appl. Math. Nonlinear Sci.* **2018**, *3*, 353–374. [CrossRef]
34. Baskonus, H.M.; Bulut, H.; Sulaiman, T.A. New Complex Hyperbolic Structures to the Lonngren-Wave Equation by Using Sine-Gordon Expansion Method. *Appl. Math. Nonlinear Sci.* **2019**, *4*, 129–138. [CrossRef]